Comparison of the powder-in-tube processing properties of two $(Bi_{2-x}Pb_x)Sr_2Ca_2Cu_3O_{10+\delta}$ powders

Timothy P. Beales, Jo Jutson, Luc Le Lay and Michelé Mölgg

Superconductivity Group, BICC Cables Ltd, Technology Centre, Wrexham, UK, LL13 9XP

The processing and formation kinetics in air of two commercial $(Bi_{2-x}Pb_x)Sr_2Ca_2Cu_3O_{10+\delta}$ powders ($Bi_{1.87}Pb_{0.34}Sr_{1.89}Ca_{1.94}Cu_{3.00}O_{10+\delta}$ and $Bi_{1.84}Pb_{0.33}Sr_{1.84}Ca_{2.07}Cu_{3.06}O_{10+\delta}$) in a silver-sheathed tape using the powder-in-tube manufacturing technique have been investigated. The highest concentration of the $(Bi_{2-x}Pb_x)Sr_2Ca_2Cu_3O_{10+\delta}$ phase was found to occur at the ceramic/silver interface. The results over a range of times and processing temperatures were fitted to an Avrami equation. In the process range that yielded the optimum volume fraction of $(Bi_{2-x}Pb_x)Sr_2Ca_2Cu_3O_{10+\delta}$ the Avrami exponent was found to be $m = 1.2$, indicative of platelike growth. In this same region the critical current densities were found to be the maximum and showed that if the entire ceramic cross-section can be processed to have a high volume fraction of the $(Bi_{2-x}Pb_x)Sr_2Ca_2Cu_3O_{10+\delta}$ phase, then critical current densities in excess of 5×10^8 A m^{-2} should be routinely achieved. The difference in physical properties of the two powders was attributed to the different starting morphologies of the powders, which determined the properties of the final product.

The most promising high-temperature superconducting material for power engineering applications at 77 K is $(Bi_{2-x}Pb_x)Sr_2Ca_2Cu_3O_{10+\delta}$ processed in a silver sheath *via* the powder-in-tube (PIT) route.[1–6] A potential early use for such materials has been identified in power transmission cables and techno-economic studies have been carried out and demonstrator devices built in Europe, Japan and the USA.[7–9] Economic viability, however, rests on the ability to manufacture relatively cheap superconductors with a high current density (J_C)[10–12] in excess of 2×10^8 A m^{-2}. Recent results on short pressed tapes[13,14] include a self-field J_C on a selected area at 77 K of over 5×10^8 A m^{-2}. The pressing method employed to obtain these J_C values is not applicable to a long-length manufacturing process, and conventional or shear high-pressure rolling is employed to manufacture tapes in the 10–1000 m range. Using this method, J_C values are not so high, but a value of 2×10^8 A m^{-2} over 100 m has been achieved.[15] The highest J_C values have been found for materials with aligned microstructures[16] and recent studies have shown that a disproportionate amount of the current distribution is concentrated at the silver/ceramic interface.[13] The PIT process is very convoluted owing to the complex phase equilibria present during the manufacturing process in which the phases of the bismuth cuprates; 2223 [$(Bi_{2-x}Pb_x)Sr_2Ca_2Cu_3O_{10+\delta}$], 2212 [$Bi_2Sr_2CaCu_2O_{8+\delta}$ or $(Bi_{2-x}Pb_x)Sr_2CaCu_2O_{8+\delta}$] and 2201 ($Bi_2Sr_2CuO_{6+\delta}$) co-exist in an incongruent system along with other liquid/semi-liquid phases of binary oxides such as CuO and PbO and ternary oxides such as Ca_2PbO_4 or alkaline-earth-metal cuprate (AEMC) phases such as $(Sr_{1-x}Ca_x)Cu_2O_3$, $(Sr_{2-x}Ca_x)CuO_3$ and $(Sr_{14-x}Ca_x)Cu_{24}O_{41}$. As a consequence of this, the PIT results presented in the scientific literature from laboratory processed samples are not statistically capable and are of little use in designing a manufacturing route. Batch-to-batch reproducibility will be a key factor in the manufacturing process, and despite the large body of work on the PIT process, there are still many unanswered questions regarding the chemistry and phase equilibria of the formation of the $(Bi_{2-x}Pb_x)Sr_2Ca_2Cu_3O_{10+\delta}$ phase. Understanding this process will be one of the keys to the successful implementation of superconducting technology at 77 K in electrical engineering.

In order to further understanding in this area, we have investigated the formation kinetics and processing properties of two commercial $(Bi_{2-x}Pb_x)Sr_2Ca_2Cu_3O_{10+\delta}$ powders in a silver sheath. As many of the processing parameters as possible were held constant between the two powders. Therefore, both samples were processed by systematically changing the annealing temperature and time in a single thermal process cycle. In addition, all experiments were carried out in air and no intermediate mechanical stages other than initial tape formation were employed. This approach allowed the results to be analysed as a three-dimensional surface rather than the two-dimensional approach usually presented in the literature. We have paid particular attention to the formation of the $(Bi_{2-x}Pb_x)Sr_2Ca_2Cu_3O_{10+\delta}$ phase at the silver interface by use of X-ray diffractometry and correlated its effect on the electrical properties of the resulting high temperature superconducting tapes.

Experimental

Partially reacted $(Bi_{2-x}Pb_x)Sr_2Ca_2Cu_3O_{10+\delta}$ powders with a target stoichiometry of $Bi_{1.84}Pb_{0.34}Sr_{1.91}Ca_{2.03}Cu_{3.06}0_{10+\delta}$ were obtained from two commercial suppliers. Powder 1 was manufactured by Merck Ltd. using a spray-pyrolysis technique and powder 2 was manufactured by Solvay GmbH using a solid state method. Both powders had received a pre-delivery annealing at temperatures in the range 750–820 °C in air.

To manufacture the PIT samples, the precursor powder was packed into a round pure silver tube (99.99%) with dimensions o.d. = 10 mm, i.d. = 8 mm and length = 150 mm with one end sealed. After loading, the packing end was closed, swaged and subjected to a series of drawing reductions to form a ceramic/metal composite wire with an inner ceramic core and outer metallic sheath. The wire was drawn down from an initial diameter of o.d. = 10 mm to a final diameter of o.d. = 1 mm using a reduction of 10% per die pass. The wire was then rolled into a tape, using a reduction of 10% in area per pass to a final thickness near to 0.2 mm. PIT processing samples with dimensions 100 mm × 2.5 mm × 0.12 mm were cut from the tape feedstock for experimental use. Measurements on the tape samples after mechanical deformation showed that the tape samples had overall transverse cross-sectional areas of 0.11 ± 0.04 mm^2 and a ceramic core thickness of 0.07 ± 0.01 mm.

Samples containing powder 1 were annealed at $820 \leqslant T/°C \leqslant 854$ for times $20 \leqslant t/h \leqslant 200$ in air, in a modified muffle furnace fitted with a specially designed internal ceramic shield for thermal stability. The samples were laid flat on an alumina

plate and placed at the centre of the furnace. Thermal calibration was carried out using a two-dimensional array of nine type N thermocouples. The temperature homogeneity was found to be ± 1 °C in a 100×100 mm plane. Samples containing powder 2 were annealed at $810 \leqslant T/°C \leqslant 846$ for times $2 \leqslant t/h \leqslant 200$ in air, in a horizontal three-zone furnace fitted with an isothermal heat pipe. The samples were laid flat on alumina plates placed at the centre of the furnace hot zone. Thermal calibration was carried out using a type R thermocouple, and temperature homogeneity was found to be better than ± 0.2 °C over a central heated zone of 350 mm.

Both powders and tapes were analysed for routine sample purity and accurate lattice parameter values, determined by X-ray powder diffraction (XRD) on a Siemens D500 powder diffractometer using a Bragg–Brentano geometry and Co-Kα radiation. The tape specimens were prepared by peeling back one side of the silver sheath (for interfacial measurements at the metal/ceramic interface, the X-ray patterns were obtained for the first 5 μm into the ceramic core). The angular range covered was $4 \leqslant 2\theta/° \leqslant 80$ using a step size $2\theta = 0.02°$ and a step time of 5 s. In addition, the angular ranges $25 \leqslant 2\theta/° \leqslant 30$ and $32 \leqslant 2\theta/° \leqslant 35$ were covered with an increased step time of 50 s to perform quantitative analysis by peak profile fitting. For ease of analysis, the Co-Kα XRD patterns were converted to those expected using Cu-Kα_1 radiation for comparison with patterns in the JCPDS database.

Combined thermogravimetry and differential thermal analysis (TG–DTA) on *ca.* 20 mg samples was carried out using a Stanton Redcroft 780 thermal analyser in flowing synthetic air (21% O_2 in N_2) or in a reduced oxygen mixture of synthetic 8% O_2 in N_2, supplied directly from a commercial gas cylinder (Air Products). Data were taken by heating the samples at 15 K min^{-1} to 750 °C and then at 4 K min^{-1} to 900 °C.

Tape samples were further analysed by back-scattered and secondary-emission scanning electron microscopy (SEM-BS and SEM-SE) using an Hitachi-S2400 electron microscope and elemental mapping by EDX analyses using a JEOL JSM-35 electron microscope. The 50 mm samples were prepared by mounting in epoxy resin and mechanically polished without any chemical etching.

Current–voltage (I–V) characteristics of tape samples at 77 K were determined over a distance between current contacts of 100 mm using a four-point technique with voltage contacts spaced 50 mm apart. The dc critical current value (I_C) was determined using a voltage criterion of 0.1 μV mm^{-1}. The critical current density (J_C) was calculated from I_C/s, where s is the superconductor cross-sectional area in the ceramic core, and was calculated using an Optimas image analysis software package connected to an Olympus optical microscope.

Results and Discussion

Pre-annealed powders

Cation stoichiometry of both powders was checked using inductively coupled plasma–atomic emission spectroscopy (ICP–AES). Powder 1 was found to have an actual cation stoichiometry of $Bi_{1.87}Pb_{0.34}Sr_{1.89}Ca_{1.94}Cu_{3.00}O_{10+\delta}$ (a higher bismuth and a lower strontium and calcium content than the target composition), and powder 2 was found to have an actual cation stoichiometry of $Bi_{1.84}Pb_{0.33}Sr_{1.84}Ca_{2.07}Cu_{3.06}O_{10+\delta}$ (a slightly lower strontium and lead content and higher calcium content than the target composition). However, both compositions are still within the phase pure region of the $(Bi_{2-x}Pb_x)Sr_2Ca_2Cu_3O_{10+\delta}$ phase diagram.[17–20] The carbon content of both powders (as CO_3^{2-}) was below 500 ppm. Particle size analysis showed that powder 1 had a d_{50} value of 4 ± 3 μm, with 10% of the powder in the range 10–20 μm. Powder 2 had a d_{50} value of 1.9 μm with the upper 10% of the powder in the range 4–7 μm. Figs. 1 and 2 show the XRD

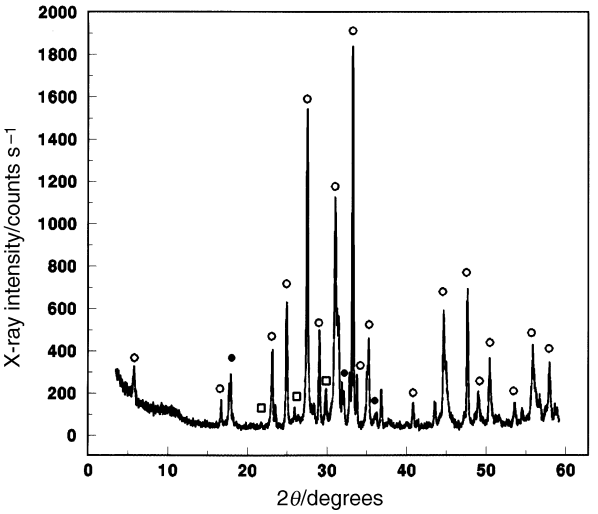

Fig. 1 XRD data for as-received powder 1 (Merck). ○, $Bi_2Sr_2CaCu_2O_{8+\delta}$; □, $Bi_2Sr_2CuO_{6+\delta}$; ●, Ca_2PbO_4.

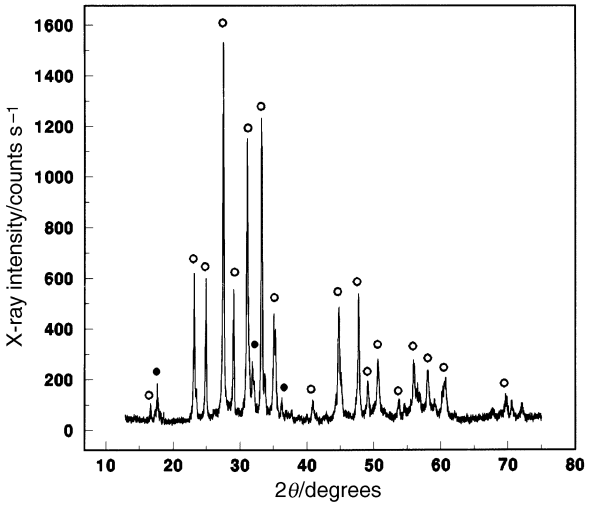

Fig. 2 XRD data for as-received powder 2 (Solvay). ○, $Bi_2Sr_2CaCu_2O_{8+\delta}$; ●, Ca_2PbO_4.

data collected over the range $5 \leqslant 2\theta/° \leqslant 70$ for the as-received powders 1 and 2 respectively. From Fig. 1, the majority phase in powder 1 was found to be $Bi_2Sr_2CaCu_2O_{8+\delta}$ with minor peaks identified as from Ca_2PbO_4, $Bi_2Sr_2CuO_{6+\delta}$ along with some unidentified peaks. Fig. 2 shows that in powder 2 the dominant phase was $Bi_2Sr_2CaCu_2O_{8+\delta}$, with minor peaks identified as belonging to Ca_2PbO_4. No $Bi_2Sr_2CuO_{6+\delta}$ peaks were observed in the as-received powder 2, in contrast to those seen in powder 1. In both samples, no $(Bi_{2-x}Pb_x)Sr_2Ca_2Cu_3O_{10+\delta}$ peaks could be identified in the XRD patterns at this stage.

XRD analysis of both powders at the surface of the tape prior to annealing showed that the $Bi_2Sr_2CaCu_2O_{8+\delta}$ ($00l$) peaks increased in relative intensity and that the secondary phases had drastically reduced in intensity when compared to the as-received powders. This implied that the $Bi_2Sr_2CaCu_2O_{8+\delta}$ grains had achieved strong a–b axis alignment by cold working relative to the other phases, and that the mechanical processing had either destroyed any larger crystallites and/or caused these phases to flow away from the silver/ceramic interface. Comparison of the increase in the ($00l$) with the decrease in (hkl) peaks (with $h \neq 0$ or $k \neq 0$) showed that the $Bi_2Sr_2CaCu_2O_{8+\delta}$ c axis alignment normal to the width of the tape was less pronounced. Using our mechanical reduction procedure, no XRD line broadening or increase in

amorphous phases was observed, contrary to that reported by others.[21]

Formation kinetics of $Bi_2Sr_2CuO_{6+\delta}$, $Bi_2Sr_2CaCu_2O_{8+\delta}$ and $(Bi_{2-x}Pb_x)Sr_2Ca_2Cu_3O_{10+\delta}$

Processing temperatures were determined after DTA analysis of the tape samples. For example, Fig. 3 shows the differential thermograms of (*a*) as-received powder 1 heated in 21% O_2 in N_2, (*b*) the same powder in the silver sheath after the first mechanical processing by heating in 21% O_2 in N_2 at 4 K min^{-1} and (*c*) the same powder in the silver sheath processed after the first mechanical deformation by heating in 8% O_2 in N_2. Analysis of trace (*a*) showed an endothermic reaction with its onset at 825 ± 1 °C, associated with a liquid-phase formation and a second endothermic peak with a shoulder at 853 ± 2 °C which corresponds to the incongruent melting of $(Bi_{2-x}Pb_x)Sr_2Ca_2Cu_3O_{10+\delta}$.[22] It is the temperature range between the first endotherm (liquid-phase formation) and the second endotherm [decomposition of $(Bi_{2-x}Pb_x)Sr_2Ca_2Cu_3O_{10+\delta}$] that defines the operational temperature window for processing. The effect of the silver sheath is seen from the middle curve in Fig. 3. In this case the reaction endotherms are (*i*) moved *ca.* −20 °C in temperature and (*ii*) broadened and the fine structure smoothed when compared to the powder processed alone. The lower trace in Fig. 3 shows that reducing the partial pressure of O_2 has the effect of lowering the temperature for the decomposition endotherm by a few degrees more. This is a much smaller effect than the presence of the silver sheath, but is significant enough to be considered an important parameter that needs controlling during processing.

The volume fractions of $Bi_2Sr_2CuO_{6+\delta}$, $Bi_2Sr_2CaCu_2O_{8+\delta}$ and $(Bi_{2-x}Pb_x)Sr_2Ca_2Cu_3O_{10+\delta}$ in the tape core were defined as F_{2201}, F_{2212} and F_{2223} and are described by eqn. (1)–(3). These were calculated by measuring the area under the most intense (*hkl*) peak of each of the above phases and dividing by the sum of these three (*hkl*) peak areas. For $Bi_2Sr_2CuO_{6+\delta}$, we used the (008) peak occurring at $2\theta=29.3°$. For $Bi_2Sr_2CaCu_2O_{8+\delta}$, we also used the (008) peak occurring at $2\theta=23.4°$ and for $(Bi_{2-x}Pb_x)Sr_2Ca_2Cu_3O_{10+\delta}$, we used the (0010) peak occurring at $2\theta=23.9°$. In addition, the conversion of $Bi_2Sr_2CaCu_2O_{8+\delta}$ into $(Bi_{2-x}Pb_x)Sr_2Ca_2Cu_3O_{10+\delta}$ was defined by C_{2223}, calculated from the volume fractions of $Bi_2Sr_2CaCu_2O_{8+\delta}$ and $(Bi_{2-x}Pb_x)Sr_2Ca_2Cu_3O_{10+\delta}$ using the (*hkl*) method described above and described by eqn. (4).

$$F_{2201}=\frac{{}_{2201}I_{(008)}}{{}_{2201}I_{(008)}+{}_{2212}I_{(008)}+{}_{2223}I_{(0010)}} \quad (1)$$

$$F_{2212}=\frac{{}_{2212}I_{(008)}}{{}_{2201}I_{(008)}+{}_{2212}I_{(008)}+{}_{2223}I_{(0010)}} \quad (2)$$

$$F_{2223}=\frac{{}_{2223}I_{(0010)}}{{}_{2201}I_{(008)}+{}_{2212}I_{(008)}+{}_{2223}I_{(0010)}} \quad (3)$$

$$C_{2223}=\frac{{}_{2223}I_{(0010)}}{{}_{2212}I_{(008)}+{}_{2223}I_{(0010)}} \quad (4)$$

F_{2201}, F_{2212}, F_{2223} and C_{2223} were calculated from the XRD patterns obtained at selected data points across the entire time–temperature matrix for tapes processed for both powders. For powder 1, the results are shown in Table 1, displaying the F_{2201}, F_{2212}, F_{2223} and C_{2223} values obtained over the entire time–temperature matrix. For powder 2, the results are shown in Table 2 (displaying the observed F_{2201}, F_{2212} and F_{2223} values with time for a set temperature of 834 °C) and Table 3 (displaying the observed F_{2201}, F_{2212} and F_{2223} values with temperature for a set time of 50 h). All three tables provide information on the formation kinetics and solid state chemistry of the bismuth cuprate system in the PIT process.

Process chemistry of $Bi_2Sr_2CuO_{6+\delta}$

Powder 1 and powder 2 exhibit different behaviour regarding the formation of $Bi_2Sr_2CuO_{6+\delta}$. For both powders at times <30 h, the volume fraction of $Bi_2Sr_2CuO_{6+\delta}$ observed at the silver/ceramic interface was negligible. For powder 1, F_{2201} appeared relatively insensitive to the processing temperature until *ca.* 828 °C, after which F_{2201} began to rise, remaining at 0.12 ± 0.02 at both short (40 h) and long (100 h) processing times. For powder 2, the value of F_{2201} at 810 °C was *ca.* 0.0; however, this was observed to rise steadily up to 0.12 at 846 °C.

Process chemistry of $Bi_2Sr_2CaCu_2O_{8+\delta}$

Again, both powder 1 and powder 2 showed different behaviour regarding the phase formation and transformation kinetics of the $Bi_2Sr_2CaCu_2O_{8+\delta}$ phase, and this was more marked at the silver/ceramic interface than that observed for the $Bi_2Sr_2CuO_{6+\delta}$ phase. For both powders, F_{2212} was high at the lower temperature range and then decreased rapidly up to a processing temperature of *ca.* 830 °C. In powder 2, at temperatures above 830 °C, F_{2212} was *ca.* 0.0 and remained negligible. In powder 1, F_{2212} was observed to fall to a certain value and then began to rise again. This behaviour was sensitive to both temperature and processing time.

Process chemistry of $(Bi_{2-x}Pb_x)Sr_2Ca_2Cu_3O_{10+\delta}$

Below 810 °C, F_{2223} was observed to be a very low value for both powders, but for a small rise in the processing temperature, a sudden rise in F_{2223} was observed and by 828 °C, for both powders F_{2223} was in the range 0.8–0.9. Once F_{2223} reached its maximum, a short plateau was observed and then F_{2223} slowly declined with increasing temperature up to 850 °C. At temperatures above 850 °C, F_{2223} fell dramatically to zero as the $(Bi_{2-x}Pb_x)Sr_2Ca_2Cu_3O_{10+\delta}$ decomposed (see Fig. 3). This temperature-stable maximum value of F_{2223} was reached between 40 and 50 h processing time for both powders, and outside this stable region, the value of F_{2223} was very sensitive to the processing temperature. The sharply declining F_{2212} values up to 830 °C and the corresponding large increases in F_{2223} values up to 850 °C imply a rapid conversion of $Bi_2Sr_2CaCu_2O_{8+\delta}$ into $(Bi_{2-x}Pb_x)Sr_2Ca_2Cu_3O_{10+\delta}$. The phase conversion, C_{2223}, at the ceramic surface was also monitored as a function of the processing temperature and time. For

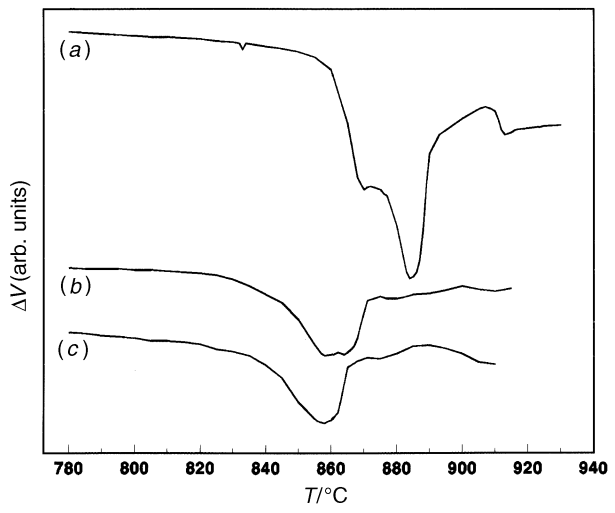

Fig. 3 DTA data of powder 1 as (*a*) as-received powder heated in 21% O_2:N_2, (*b*) in an Ag sheath after the first mechanical deformation heated in 21% O_2 in N_2 and (*c*) in an Ag sheath after the first mechanical deformation heated in 8% O_2 in N_2

Table 1 Observed F_{2201}, F_{2212}, F_{2223} and C_{2223} values over the entire time–temperature matrix for a tape processed with powder 1

	$t=20$ h				$t=40$ h				$t=60$ h				$t=100$ h			
T/°C	F_{2201}	F_{2212}	F_{2223}	C_{2223}	F_{2201}	F_{2212}	F_{2223}	C_{2223}	F_{2201}	F_{2212}	F_{2223}	C_{2223}	F_{2201}	F_{2212}	F_{2223}	C_{2223}
820	—	—	—	—	—	—	—	—	—	—	—	—	n.d.[a]	0.762	0.238	0.238
828	—	—	—	—	n.d.[a]	0.145	0.855	0.855	—	—	—	—	n.d.[a]	0.145	0.855	0.855
832	—	—	—	—	0.085	0.132	0.781	0.855	—	—	—	—	0.111	0.031	0.858	0.965
834	—	0.615	0.385	0.358	0.129	0.088	0.783	0.899	0.119	0.045	0.835	0.949	0.108	0.035	0.857	0.961
838	—	0.399	0.60	0.601	0.095	0.136	0.769	0.850	0.077	0.076	0.851	0.918	0.114	0.036	0.849	0.959
842	—	0.466	0.534	0.534	0.104	0.171	0.724	0.809	0.130	0.085	0.784	0.902	0.133	0.061	0.806	0.930
850	—	—	—	—	0.148	0.240	0.612	0.718	—	—	—	—	—	—	—	—

[a]n.d. = not determined.

Table 2 Observed F_{2201}, F_{2212}, F_{2223} and C_{2223} values with time for a tape containing powder 2 processed at 834 °C

	processing time/h							
	8	15	24	48	72	98	120	200
F_{2201}	0.086	0.080	0.064	0.078	0.095	0.066	0.088	0.058
F_{2212}	0.618	0.267	0.116	0.001	0.0	0.0	0.0	0.0
F_{2223}	0.296	0.653	0.820	0.921	0.905	0.934	0.912	0.942
C_{2223}	0.324	0.709	0.876	0.953	0.999	1.00	1.00	1.00

example, in tapes containing powder 2, processed at 834 °C, for $0 \leqslant t/\text{h} \leqslant 120$, it was found that after only 2 h $C_{2223}=0.135$ which increased rapidly to 0.709 by 15 h. After 48 h, $C_{2223}=0.99$.

The results obtained for this type of solid state conversion can be fitted to the Avrami equation.

$$\alpha = 1-\exp(-kt^m) \quad (5)$$

where α is the phase concentration at time t (*i.e.* C_{2223}) and k and m are constants. The value of m can provide an indication of the reaction mechanism. Fig. 4 shows a plot of $\log.\log[1/(1-C_{2223})]$ *vs.* $\log t$ for processed tape samples containing both powder 1 and powder 2 for a series of annealing temperatures. A straight line is obtained in each case, with gradient m. At the processing temperature of 834 °C the data for both powder 1 and powder 2 give a value of $m=1.2$. For other temperatures this value of m changes, *e.g.* for powder 1 at 838 °C, $m=0.78$ and at 842 °C, $m=0.80$. A theoretical approach by Hulbert[23] showed values in the range $1 \leqslant m \leqslant 2$ are indicative of a two-dimensional, platelike growth mechanism.

The observed C_{2223} values at a defined temperature were found to increase sharply with time, eventually reaching a finite limit just below the theoretical maximum of 1.0 at a characteristic time. For example, the data for powder 2 in Fig. 4 can be fitted exactly to the equation $C_{2223}=1-\exp(-4.4\times10^{-2}\ t^{1.23})$. By plotting the observed C_{2223} values over the whole time and temperature matrix, it can be seen that C_{2223} exists as a plateau with steep slopes on either side, as shown in Fig. 5. This data was obtained using powder 1, but an almost identical surface is also seen with powder 2 samples. Using Fig. 5, we can analyse the effect of temperature by following a particular time contour. For example, at 100 h, the maximum value of C_{2223} (0.96) occurs within a narrow temperature window of 835 ± 3 °C.

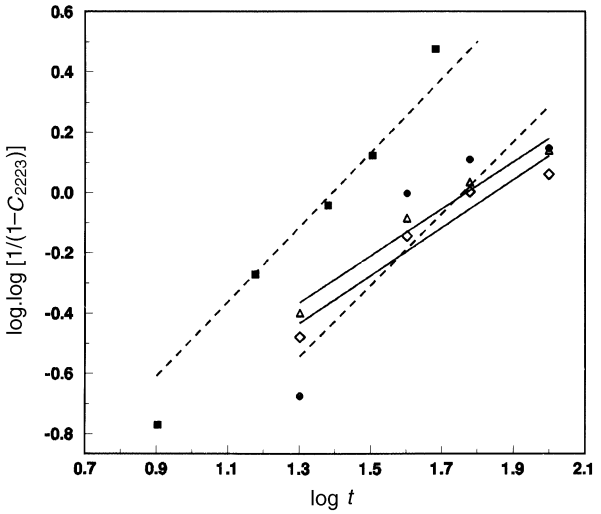

Fig. 4 Plots of $\log.\log[1/(1-C_{2223})]$ *vs.* $\log t$ for tape samples made with powder 1 and powder 2. ●, ——, sample 1 processed at 834 °C; ■, ---, sample 2 processed at 834 °C; △, —, sample 1 processed at 838 °C; ◇, —, sample 1 processed at 842 °C.

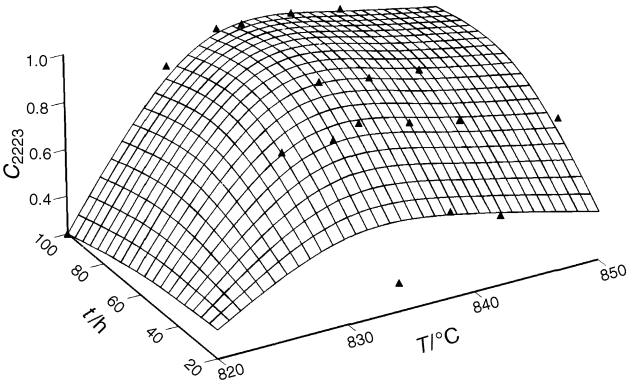

Fig. 5 A three-dimensional plot of C_{2223} *vs.* processing temperature and time showing a reaction surface for a tape containing powder 1 (data = ▲)

Table 3 Observed F_{2201}, F_{2212} and F_{2223} values at a set time of 50 h with processing temperature for a tape containing powder 2

	processing temperature/°C											
	810	820	825	826	828	830	832	834	836	838	842	846
F_{2201}	0.00	0.037	0.049	0.052	0.060	0.060	0.055	0.066	0.099	0.089	0.117	0.122
F_{2212}	0.114	0.067	0.026	0.015	0.004	0.002	0.001	0.000	0.000	0.001	trace	trace
F_{2223}	0.886	0.895	0.925	0.933	0.936	0.938	0.945	0.934	0.901	0.915	0.882	0.878

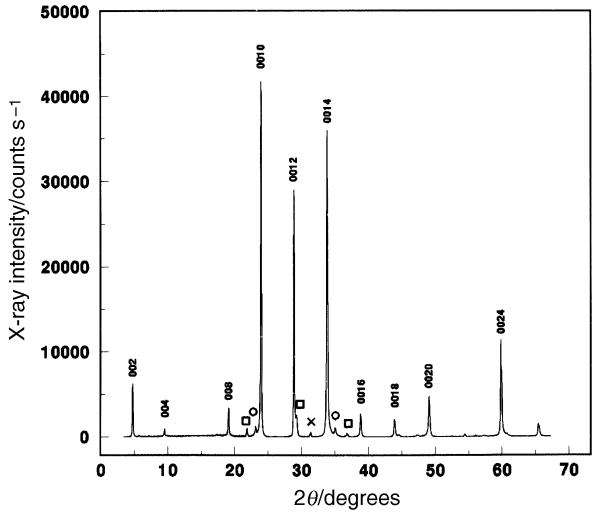

Fig. 6 XRD data for the ceramic surface of a tape containing powder 1 processed at 834 °C for 100 h. Main phase $(Bi_{2-x}Pb_x)Sr_2Ca_2Cu_3O_{10+\delta}$; ○, $Bi_2Sr_2CaCu_2O_{8+\delta}$; □, $Bi_2Sr_2CuO_{6+\delta}$; ×, AEMC.

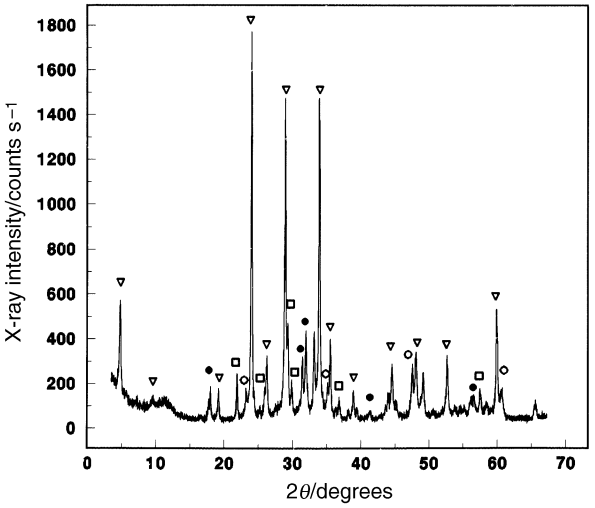

Fig. 7 XRD data for the ceramic core of a tape containing powder 1 processed at 834 °C for 100 h. The (00*l*) peaks of $(Bi_{2-x}Pb_x)Sr_2Ca_2Cu_3O_{10+\delta}$ are identified ▽, along with ○, $Bi_2Sr_2CaCu_2O_{8+\delta}$; □, $Bi_2Sr_2CuO_{6+\delta}$; ●, Ca_2PbO_4.

Physical properties

Fig. 6 shows the XRD patterns of the ceramic/silver interface from peeled tape samples processed with powder 1, after annealing at 834 °C for 100 h in air. The (00*l*) peaks belonging to the phases present are identified. $Bi_2Sr_2CuO_{6+\delta}$ peaks are indicated with open squares [the strongest peaks, (006), (008) and (0010), occur at $2\theta = 21.8$, 29.2 and 36.8° respectively]; $Bi_2Sr_2CaCu_2O_{8+\delta}$ are identified with open circles [the strongest peaks, (008) and (0012) occur at $2\theta = 23.04$ and 34.94° respectively] and $(Bi_{2-x}Pb_x)Sr_2Ca_2Cu_3O_{10+\delta}$ peaks are identified [the strongest peaks (0010), (0012) and (0014) occur at $2\theta = 23.91$, 28.83 and 33.80° respectively]. In addition, low intensity peaks characteristic of Ca_2PbO_4 and the alkaline-earth-metal cuprate (AEMC) phases could also be identified (shown with an × in Fig. 6). For tapes processed with powder 2, also annealed at 834 °C, a very similar XRD pattern of the ceramic/silver interface from peeled tape samples compared to Fig. 6 is observed. For powder 2, the majority phase present was found to be $(Bi_{2-x}Pb_x)Sr_2Ca_2Cu_3O_{10+\delta}$, with some $Bi_2Sr_2CuO_{6+\delta}$ and a small quantity of $Bi_2Sr_2CaCu_2O_{8+\delta}$.

C_{2223} was found to have its maximum value at the ceramic/silver interface for tape samples containing both powders, and decreased with distance in moving away from the silver interface towards the centre of the tape. To investigate this further, the surface ceramic layers were systematically removed in 20–30 μm steps by careful mechanical grinding of the ceramic away from the metal interface and into the core. The XRD patterns from these layers showed a marked contrast to those obtained from the silver interface. The volume fractions of $Bi_2Sr_2CuO_{6+\delta}$ and $Bi_2Sr_2CaCu_2O_{8+\delta}$, were higher ($F_{2201}$ increased from 0.103 to 0.239 and F_{2212} increased from 0.035 to 0.056) and the volume fractions of both Ca_2PbO_4 and AEMC phases were also markedly increased. C_{2223} was found to correspondingly decrease from 0.957 to 0.926. To obtain further information on the total phase composition of the core, the entire ceramic core was removed from the silver sheath after processing and analysed as a powder by XRD. Fig. 7 shows a typical XRD pattern of powder 1 removed from its silver sheath after processing at 834 °C for 100 h. In contrast with the interfacial XRD of Fig. 6, the total core composition shows the majority phase to be $(Bi_{2-x}Pb_x)Sr_2Ca_2Cu_3O_{10+\delta}$, but also the presence of significant concentrations of Ca_2PbO_4, $Bi_2Sr_2CuO_{6+\delta}$, $Bi_2Sr_2CaCu_2O_{8+\delta}$ and AEMC phases.

SEM-BS images of polished transverse cross-sections show the platelike grains of $(Bi_{2-x}Pb_x)Sr_2Ca_2Cu_3O_{10+\delta}$ physically aligned with the silver surface in the interface region. Further into the core, $(Bi_{2-x}Pb_x)Sr_2Ca_2Cu_3O_{10+\delta}$ grains were observed to have a more random orientation, especially around AEMC grains, suggesting that the local $(Bi_{2-x}Pb_x)Sr_2Ca_2Cu_3O_{10+\delta}$ grain orientation was strongly influenced by the surrounding ceramic matrix with the corresponding loss of the high orientation achieved at the silver interface. EDX analysis showed that the cation stoichiometry of the AEMC phases was either $(Sr,Ca)_2CuO_3$ or $(Sr,Ca)_{14}Cu_{24}O_{41}$, and both were strontium-rich. Fig. 8 shows a typical micrograph of a tape processed at 834 °C for 40 h. The central area is a longitudinal cross-section of the ceramic core and the silver sheath can be seen on either side. The dark areas are either AEMC, Ca_2PbO_4 or voids, the light streaks are $Bi_2Sr_2CaCu_2O_{8+\delta}$ and the grey is $(Bi_{2-x}Pb_x)Sr_2Ca_2Cu_3O_{10+\delta}$. The increased *c*-axis texturing can be seen at the silver/ceramic interface.

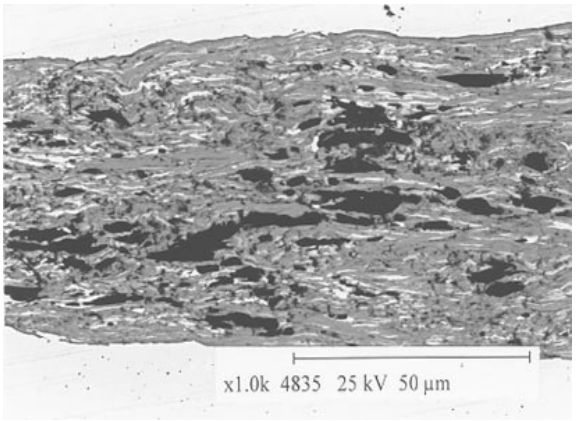

Fig. 8 An SEM-BS micrograph of a tape processed at 834 °C for 40 h in air. The silver sheath is at the top and bottom. The various phase distribution can be identified as dark grey = $(Bi_{2-x}Pb_x)Sr_2Ca_2Cu_3O_{10+\delta}$, light grey = $Bi_2Sr_2CaCu_2O_{8+\delta}$ and black = Ca_2PbO_4, AEMC or void.

The difference observed by XRD in composition between the ceramic at the silver interface and in the tape core can be ascribed to two different reasons. The first is mechanical. Like $(Bi_{2-x}Pb_x)Sr_2Ca_2Cu_3O_{10+\delta}$, $Bi_2Sr_2CaCu_2O_{8+\delta}$ has a micaceous morphology and as a consequence of the mechanical processing prior to annealing, the $Bi_2Sr_2CaCu_2O_{8+\delta}$ plates present as the majority phase in the starting powders are preferentially aligned at the interface by the mechanical stresses in forming a flat tape from a round wire. This is observed in

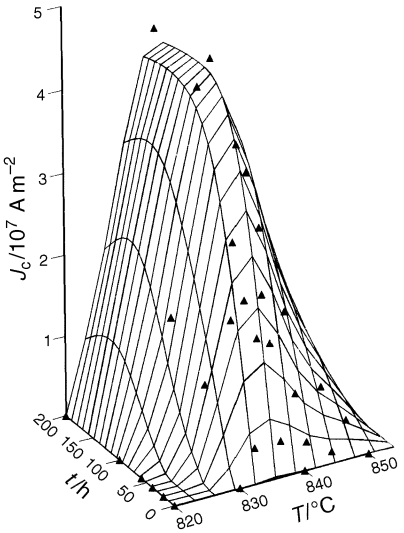

Fig. 9 A three-dimensional plot of J_C *vs.* processing temperature and time showing a reaction surface for a tape containing powder 1 (data = ▲)

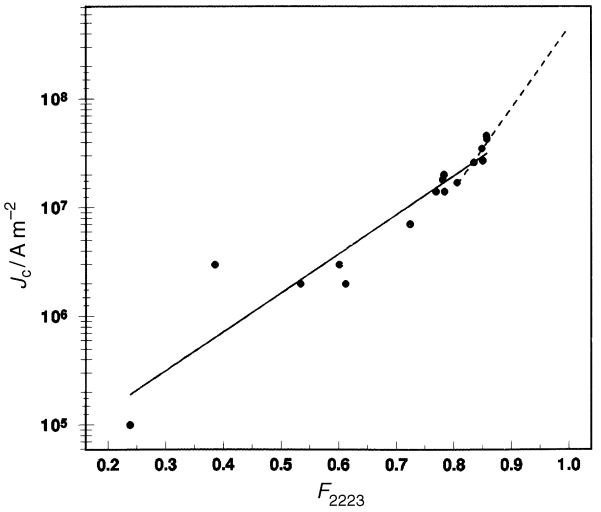

Fig. 10 A plot of J_C (log scale) *vs.* F_{2223}. The change in gradient at $F_{2223} \approx 0.8$ suggests that J_C values in excess of 5×10^8 A m^{-2} should be attainable if the entire core can be processed with $F_{2223} \approx 1.0$.

the pre-annealed XRD patterns. Our results suggest that the other phases present are forced away from the interfacial region by plastic flow and their relative concentration increases at the ceramic core, towards the region of least mechanical work. Once thermal processing begins, F_{2223} is bound to be higher at the interface owing to the higher concentration of $Bi_2Sr_2CaCu_2O_{8+\delta}$ already present there. The second reason may be chemical in nature and related to the presence of silver. Our DTA measurements show that the presence of silver and the ambient atmosphere can reduce the reaction endotherm peaks by as much as 24 °C when compared to the powder alone in air. This, and possible capillary action on the liquidus, may also account for the higher volume fraction of $(Bi_{2-x}Pb_x)Sr_2Ca_2Cu_3O_{10+\delta}$ at the interface as this region has the highest contact surface area between the ceramic and silver, allowing easier formation from the $Bi_2Sr_2CaCu_2O_{8+\delta}$ grains. A smaller effect may also arise from the fact that silver is known to be permeable to oxygen, especially at elevated temperatures which again may favour $(Bi_{2-x}Pb_x)Sr_2Ca_2Cu_3O_{10+\delta}$ at the interface rather than the core where the partial pressure of O_2 would be expected to be lower.

Further PIT tape samples were processed using the matrix described above and these were electrically characterised by determining the self-field J_C at 77 K. A three-dimensional plot of the observed J_C as a function of annealing temperature and time for PIT samples using powder 1 is shown in Fig. 9. Below processing temperatures of 820 °C and above 854 °C, all the tape samples were resistive and showed ohmic behaviour. Under the processing conditions in this experiment, J_C was found to exhibit its maximum value within the narrow temperature range 835 ± 3 °C. This range corresponds to the same temperature in Fig. 5 where both F_{2223} and C_{2223} respectively showed their maximum values. From Fig. 9, it can be seen that J_C is very sensitive to the processing parameters. Above a processing time of 100 h, a deviation of ± 2 °C from the optimum 834 °C results in a 25% drop in J_C from its maximum value. The increase in J_C with F_{2223} is of the form of an exponential increase with a very sharp rise at values of $F_{2223} > 0.8$. These data are shown in Fig. 10, re-plotted from Fig. 9 as a two-dimensional plot of the observed J_C (log scale) *vs.* F_{2223}, which expresses the data in a linear form, and it is clear that high J_C values correspond to high F_{2223} values. From this graph, the change of slope at $F_{2223} = 0.8$ is seen as a change of gradient. By extrapolating to $F_{2223} = 1.0$, we can predict that if the entire core resembled the F_{2223} values seen at the silver/ceramic interface then J_C values in excess of 5×10^8 A m^{-2} should be attained. The J_C measurement only considers the entire cross-sectional area where F_{2223} is far from optimum. At the interface, F_{2223} is very close to 1.0 and so J_C in this region of the tape must be very high. This phenomenon has been studied by Larbalestier *et al.*,[13] who performed intricate J_C measurements on microsections of a PIT processed tape, cut sequentially from the interface and into the core. Our data support their conclusions of a very high J_C concentrated at the tape edges which accounts for a large proportion of the supercurrent in the tape.

Phase equilibria of $Bi_2Sr_2CuO_{6+\delta}$, $Bi_2Sr_2CaCu_2O_{8+\delta}$ and $(Bi_{2-x}Pb_x)Sr_2Ca_2Cu_3O_{10+\delta}$

Chen and Stevenson proposed[24] that $Bi_2Sr_2CaCu_2O_{8+\delta}$ reacts with liquid-phase Ca_2PbO_4, decomposing into $Bi_2Sr_2CuO_{6+\delta}$ as an intermediary which then reacts further with liquidus Ca^{2+} and Cu^{2+} salts to form $(Bi_{2-x}Pb_x)Sr_2Ca_2Cu_3O_{10+\delta}$. Although the presence of a liquid phase in this phase equilibrium is well known,[24,25] this mechanism cannot be correct from the volume fraction values found in this study. Hornung *et al.*[26] studied the *in situ* formation of $(Bi_{2-x}Pb_x)Sr_2Ca_2Cu_3O_{10+\delta}$ on open silver ribbons by XRD and found different volume fractions and phase equilibria to those found in our study. We believe that in the Hornung experiment, the powder stoichiometry was not fully under control as excess PbO pellets were needed to compensate for the highly volatile Pb loss from $(Bi_{2-x}Pb_x)Sr_2Ca_2Cu_3O_{10+\delta}$ in the open ribbons at high temperatures. This could easily account for the different volume fractions observed from our work. Other studies on PIT processed samples by Luo *et al.*[27] studied the whole core but did not compare it with the interface. Again, any differences in phase compositions reported by these workers can be explained by the fact that they used a different powder stoichiometry ($Bi_{1.84}Pb_{0.34}Sr_{1.91}Ca_{2.03}Cu_{3.06}0_{10+\delta}$) and processed the powders in a reduced oxygen atmosphere (7.5% O_2 in N_2). In addition, Luo *et al.*[27] reported evidence of mechanical damage and (00*l*) peak broadening during the pre-annealing mechanical deformation stage, and the presence of $(Sr,Ca)_{14}Cu_{24}O_{41}$ and $(Ca,Sr)_2CuO_3$ phases at the ceramic/silver interface in the annealed tape. Neither of these were seen in this study.

Our results suggest that, while $Bi_2Sr_2CaCu_2O_{8+\delta}$ in contact with the liquid phase is unstable at temperatures above 800 °C, it can decompose in two possible ways. The first route is the rapid reaction of $Bi_2Sr_2CaCu_2O_{8+\delta}$ with the liquid phase to

form $(Bi_{2-x}Pb_x)Sr_2Ca_2Cu_3O_{10+\delta}$ with the intercalation of Pb^{2+}, Ca^{2+} and Cu^{2+} into $Bi_2Sr_2CaCu_2O_{8+\delta}$ to form $(Bi_{2-x}Pb_x)Sr_2Ca_2Cu_3O_{10+\delta}$ in a diffusion-controlled process [evidence that Pb can intercalate into $Bi_2Sr_2CaCu_2O_{8+\delta}$ comes from the identification of a metastable intermediate $(Bi_{2-x}Pb_x)Sr_2CaCu_2O_{8+\delta}$, by powder XRD[28]]. Initially, the high $Bi_2Sr_2CaCu_2O_{8+\delta}$: liquid ratio allows the rapid formation of $(Bi_{2-x}Pb_x)Sr_2Ca_2Cu_3O_{10+\delta}$, with the rate progressively slowing as the $Bi_2Sr_2CaCu_2O_{8+\delta}$: liquid ratio falls and the concentration of $(Bi_{2-x}Pb_x)Sr_2Ca_2Cu_3O_{10+\delta}$ increases. The second decomposition route for $Bi_2Sr_2CaCu_2O_{8+\delta}$ is into $Bi_2Sr_2CuO_{6+\delta}$ and liquid phase. Our data suggests that this is a slow reaction and that any $Bi_2Sr_2CuO_{6+\delta}$ formed by this route is thermodynamically stable. This explains the observation of small concentrations of $Bi_2Sr_2CuO_{6+\delta}$ over the entire temperature range in this study and in others.[29] It also suggests that $Bi_2Sr_2CuO_{6+\delta}$ does not rapidly re-react with the liquid phase to re-form $Bi_2Sr_2CaCu_2O_{8+\delta}$.

Conclusions

We have systematically studied and identified the processing parameters that affect the superconducting properties for two different $Bi_{1.84}Pb_{0.33}Sr_{1.84}Ca_{2.07}Cu_{3.06}$ powders processed as silver PIT tapes. We were able to ascertain that the different physico-chemical characteristics observed were primarily due to the different morphologies of the starting powders. For both powders, platelike growth of $(Bi_{2-x}Pb_x)Sr_2Ca_2Cu_3O_{10+\delta}$ arose from a rapid diffusion-controlled reaction of $Bi_2Sr_2CaCu_2O_{8+\delta}$ with a liquid phase at temperatures above 830 °C. $Bi_2Sr_2CaCu_2O_{8+\delta}$ can also decompose to form thermodynamically stable $Bi_2Sr_2CuO_{6+\delta}$ *via* a much slower reaction. The highest concentration of $(Bi_{2-x}Pb_x)Sr_2Ca_2Cu_3O_{10+\delta}$ occurs at the silver/ceramic interface, which is due to the mechanical distribution of the starting powder. The plastic flow of the ceramic core during the initial wire formation concentrates and *c*-axially aligns $Bi_2Sr_2CaCu_2O_{8+\delta}$ at the interface. This results in an uneven critical current distribution in the core, with the highest critical current occurring at the silver/ceramic interface.

This work was supported by BICC Cables Ltd and the European Union under contract BRE2-CT93–3035.

References

1 K. H. Sandhage, G. N. Riley Jr. and W. L. Carter, *J. Met*., 1991, **43**, 21.
2 K. Sato, *Phys. World*, 1992, **5**, 37.
3 T. P. Beales, L. Le Lay, M. Mölgg, C. Ferrari and W. Segir, *Nuovo Cimento D*, 1994, **16**, 2067.
4 M. J. Minot, D. Buczek, J. J. Gannon, P. K. Miles, D. R. Parker and P. Metra, *IEEE Trans. Appl. Supercond*., 1995, **5**, 1246.
5 H. Krauth, J. Tenbrink, H-W. Neumüller, M. Wilhelm, K. Fischer, M. Schubert, W. Goldacker and J. Kessler, in *Proc. EUCAS 93*, ed. H. C. Freyhardt, DGM Informationsgesellschaft, Göttingen, Germany, 1993, p. 147.
6 J. Tenbrink, M. Wilhelm, K. Heine and H. Krauth, *IEEE Trans. Magn*., 1991, **27**, 1239.
7 T. P. Beales, C. M. Friend, L. Le Lay, M. Mölgg, C. Dineen, D. M. Jacobson, S. R. Hall, M. R. Harrison, P. F. Hermann, A. Petitbon, P. Carracino, L. Gherardi, P. Metra, G. Bognor and H-W. Neumüller, *Supercond. Sci. Technol*., 1995, **8**, 909.
8 C. M. Friend, I. Ferguson, I. W. Kay, L. Le Lay, M. Mölgg, C. Groombridge and T. P. Beales, in *Applied Superconductivity 1995*, IOP Conference Series No. 148(1), ed. D Dew-Hughes, IOP, Bristol, 1995, p. 431.
9 T. P. Beales, C. M. Friend, W. Segir, E. Ferrero, F. Vivaldi and L. Ottonello, *Supercond. Sci. Technol*., 1996, **9**, 43.
10 O. Miura, S. Tanaka, K. Miyoshi, N. Ichiyanagi, Y. Tanaka, H. Ishii and T. Hara, *Cryogenics*, 1996, **36**, 589.
11 T. P. Beales and J. S. McCormack, in *Proc. 4th World Congress on Superconductivity*, ed. K. Krishnan and C. Burnham, NASA Conference Publication 3290, Orlando, USA, 1995, p. 650.
12 S. P. Ashworth, P. Metra and R. J. Slaughter, *Eur. Trans. Elect. Power Eng*., 1994, **4**, 293.
13 D. C. Larbalestier, X. Y. Cai, Y. Feng, H. Edelman, A. Umezawa, G. N. Riley Jr. and W. L. Carter, *Physica C*, 1994, **221**, 299.
14 Q. Li, K. Brodersen, H. A. Hjuler and T. Freltoft, *Physica C*, 1993, **217**, 360.
15 M. J. Minot, W. L. Carter, J. J. Gannon Jr., R. S. Hamilton, P. K. Miles, D. R. Parker, G. N. Riley Jr., M. Rupich, M. R. Teplitsky, E. D. Thompson and K. Zafar, *Adv. Cryo. Eng*., 1994, **40**, 131.
16 K. Sato, N. Shibuta, H. Mukai, T. Hikata, M. Ueyama and T. Kato, *J. Appl. Phys*., 1991, **70**, 6484.
17 H. Maeda, Y. Tanaka, M. Fukutumi and T. Ansano, *Japn. J. Appl. Phys*., 1988, **27**, L209.
18 S. Koyama, U. Endo and T. Kawai, *Japn. J. Appl. Phys*., 1988, **27,** L1861.
19 U. Endo, S. Koyama and T. Kawai, *Japn. J. Appl. Phys*., 1989, **28,** L190.
20 K. Schulze, P. Majewski, B. Hettich and G. Petzow, *Z. Metallkd*., 1990, **81**, 836.
21 W. L. Carter, G. N. Riley Jr., J. S. Luo, N. Merchant and V. A. Maroni, *Appl. Supercond*., 1993, **1**, 1523.
22 P. Carracino, L. Gherardi, M. Catti and E. D'Acci, *Nuovo Cimento D*, 1994, **16**, 1665.
23 S. F. Hulbert, *J. Br. Ceram. Soc*., 1969, **6**, 11.
24 Y. L. Chen and R. Stevenson, *J. Am. Ceram. Soc*., 1992, **75**, 1150.
25 P. E. D. Morgan, R. M. Housley, J. R. Porter and J. J. Ratto, *Physica C*, 1991, **176**, 279.
26 R. Hornung, G. Zorn, H-W. Neumüller and G. Tomandl, *Appl. Supercond*., 1994, **2**, 337.
27 J. S. Luo, N. Merchant, E. Escorcia-Aparicio, V. A. Maroni, D. M. Gruen, B. S. Tani, G. N. Riley Jr. and W. L. Carter, *IEEE Trans. Appl. Supercond*., 1993, **3**, 972.
28 A. Jeremie, K. Alami-Yadri, J.-C. Grivel and R. Flükiger, *Supercond. Sci. Technol*., 1993, **6**, 730.
29 J. L. MacManus-Driscoll, J. C. Bravman, R. J. Savoy, G. Gorman and R. B. Beyers, *J. Am. Ceram. Soc*., 1994, **77**, 2305.

Paper 6/06896K; *Received* 8*th October*, 1996